

# Development of a Mechanics-Based Model of Brain Deformations during Intracerebral Hemorrhage Evacuation

Saramati Narasimhan<sup>1</sup>, Jared A. Weis<sup>1</sup>, Isuru S. Godage<sup>3</sup>, Robert Webster<sup>3,4</sup>, Kyle Weaver<sup>4</sup>,  
Michael I. Miga<sup>1,2,4,5</sup>

*1Vanderbilt University, Department of Biomedical Engineering, Nashville, TN USA*

*2Department of Radiology and Radiological Sciences, Vanderbilt University, Nashville, TN USA*

*3Vanderbilt University, Department of Mechanical Engineering, Nashville, TN USA*

*4Vanderbilt University Medical Center, Department of Neurological Surgery, Nashville, TN USA*

*5Vanderbilt Institute in Surgery and Engineering, Nashville, TN USA*

## ABSTRACT

Intracerebral hemorrhages (ICHs) occur in 24 out of 100,000 people annually and have high morbidity and mortality rates. The standard treatment is conservative. We hypothesize that a patient-specific, mechanical model coupled with a robotic steerable needle, used to aspirate a hematoma, would result in a minimally invasive approach to ICH management that will improve outcomes. As a preliminary study, three realizations of a tissue aspiration framework are explored within the context of a biphasic finite element model based on Biot's consolidation theory. Short-term transient effects were neglected in favor of steady state formulation. The Galerkin Method of Weighted Residuals was used to solve coupled partial differential equations using linear basis functions, and assumptions of plane strain and homogeneous isotropic properties. All aspiration models began with the application of aspiration pressure sink(s), calculated pressures and displacements, and the use of von Mises stresses within a tissue failure criterion. With respect to aspiration strategies, one model employs an element-deletion strategy followed by aspiration redeployment on the remaining grid, while the other approaches use principles of superposition on a fixed grid. While the element-deletion approach had some intuitive appeal, without incorporating a dynamic grid strategy, it evolved into a less realistic result. The superposition strategy overcame this, but would require empirical investigations to determine the optimum distribution of aspiration sinks to match material removal. While each modeling framework demonstrated some promise, the superposition method's ease of computation, ability to incorporate the surgical plan, and better similarity to existing empirical observational data, makes it favorable.

**Keyword List:** Intracerebral hemorrhage, finite element model, steerable needle, active cannula

## I. INTRODUCTION

Intracerebral hemorrhages (ICH) are the result of blood vessels within the brain rupturing. The incidence of ICH is approximately 24 out of 100,000 people a year. The median one-month mortality rate is 40%, and there is also a high incidence of morbidity [1]. ICHs make up approximately 10 to 15% of all strokes. Some primary causes of ICHs include hypertension, cerebral amyloid angiopathy, sympathomimetic drugs of abuse, and coagulopathy [2]. Uncontrolled hypertension is one of the most significant risk factors for reoccurring ICHs [3]. Treatment options include blood pressure management, coagulation management, and surgery [2]. In the INTERACT2 trial, the mortality and morbidity outcomes of patients with an ICH, less than 6 hours old, were similar between patients who underwent traditional management techniques and new intensive blood pressure lowering techniques [4]. Surgical approaches for ICH intervention have been attempted, but there has not been conclusive data showing that surgical intervention improves patient outcomes [2], [5]. Studies have also investigated treating ICHs with decompressive craniectomies. These studies revealed improved outcomes, but were limited by a small patient population [6]. Despite continuing innovations in the field, satisfactory ICH management remains a significant unsolved medical challenge.

There are investigational studies into less invasive techniques that seek to more effectively treat ICHs, but these techniques are not accepted as a standard method of treatment [7]–[9]. One proposed minimally invasive technique, which will be the focus of the model presented, is a needle-based robotic system for image-guided evacuation of ICHs [9]. The ICH robotic system consists of a sterilizable robotic actuation unit, an active cannula driven by the actuation unit, a trajectory guide, which enables the hemorrhage to be targeted using image guidance, an aspirator to evacuate the

ICH, and a passive articulated arm. The cannula consists of a precurved and superelastic inner tube, and an outer tube which is straight and stiff [9][10]. The proposed surgical workflow of this device is as follows. Preoperative computed tomography (CT) images of the patient would be obtained. Using an intraoperative scan of the patient's face, the preoperative CT will be registered into the patient space. Upon completion of the registration, the active cannula is then aligned [9]. A burr hole will be made in the skull, then the dura is opened, and the trajectory guide will be attached to the skull. Following this, the trajectory stem would then be attached to the base, and the alignment probe would then be inserted into the trajectory stem, while using the image guidance system for alignment [9]. A locking ring would then be tightened, fixing the trajectory stem into place, and once this is complete, the alignment probe would be removed [9]. The robot is then brought into the surgical field and attached to the trajectory stem. Finally, the active cannula is then passed into the brain through the trajectory stem and navigated through the ICH, based on a preplanned path. As the inner cannula is deployed, the ICH is evacuated in a systematic manner [9]. In order to limit the number of intraoperative CT scans that would need to be obtained, a mechanics based model of the evacuation of the ICH is necessary to ensure safety of the procedure.

A previous study analyzed ICH shapes using a two-dimensional (2D), finite element model, representing the ICH as six vectors radiating outwards. This study concluded that computational models could improve the clinical understanding of ICH patients [11]. Other computational models have been used to represent intraoperative events, including retraction and resection [12]. Developing a model that captures the deformations and dynamics of the surgical interaction involved with the evacuation of an ICH may be an important complement for creating minimally invasive techniques for this patient population. The combined development of a biomechanical patient-specific model and robotic platform could be an innovative guidance solution for patients suffering from an ICH. In this study, it is hypothesized that a patient specific, biomechanical model could augment an active cannula designed to access the intracerebral hemorrhage through a minimal path, and be used to guide ICH aspiration process and likely complement intraoperative imaging. The purpose of the work presented in this paper is to develop a preliminary, computational, finite element model (FEM) to represent ICH aspiration. To the best of our knowledge, this study creates the first, preliminary, computational, biomechanical model of ICH evacuation. If this work is fully realized it can ultimately be utilized with the ICH robot system described previously and reduce the number of intraoperative CT scans to which the patient would be exposed thus significantly reducing ionizing radiation exposure. In addition, if possible, reduction of intraoperative CT scans would improve clinical procedural work-flow. This work may also be extended by providing additional guidance for other minimally invasive ICH evacuation techniques in development.

## II. METHODS

### 2.1 Continuum, Finite Element Model of Brain Deformations

The model treats brain tissue as a fluid saturated poro-elastic medium [13], [14] represented by biphasic consolidation theory. The associated partial differential equations were used to calculate pressure, displacements, and von Mises stress distributions [13]–[15]. The equations for consolidation in soft-tissue can be written as [13]–[15]:

$$\nabla \cdot G \nabla \vec{u} + \nabla \frac{G}{1-2\nu} (\nabla \cdot \vec{u}) - \alpha \nabla p = 0 \quad (1a)$$

$$\alpha \frac{\partial}{\partial t} (\nabla \cdot \vec{u}) + \frac{1}{S} \frac{\partial p}{\partial t} - \nabla \cdot k \nabla p = 0 \quad (1b)$$

where

$G$	Shear modulus	(Pa)
$\vec{u}$	Displacement vector	(m)
$\nu$	Poisson's ratio	
$\alpha$	Ratio of fluid volume extracted to volume change of tissue when compressed	
$p$	Pore fluid pressure	(Pa)
$1/S$	Amount of fluid that can be forced into the tissue under a constant volume	(1/Pa)
$k$	Hydraulic conductivity	(m <sup>3</sup> s/kg).

Equation (1a) relates the mechanical equilibrium to the pressure gradient, which is treated as a body force on the control volume. Equation (1b) relates volumetric strain to the conservation of fluid in a porous media [13]–[15]. The brain is treated as a fully saturated medium,  $\alpha = 1$  and  $1/S = 0$ . In this study, the equations (1a and 1b) were simplified into their steady state forms and linear elastic mechanical behavior was employed. With these assumptions and simplifications, the governing equations of this model can be written as:

$$\nabla \cdot G \nabla \vec{u} + \nabla \frac{G}{1-2\nu} (\nabla \cdot \vec{u}) - \nabla p = 0 \quad (2a)$$

$$-\nabla \cdot k \nabla p = 0 \quad (2b)$$

Using the Galerkin Method of Weighted Residuals, the governing equations (2a and 2b) are treated using the standard weighted residual method [16].

$$\langle G \nabla \vec{u} \cdot \nabla \phi_i \rangle + \left\langle \frac{G}{1-2\nu} (\nabla \cdot \vec{u}) \nabla \phi_i \right\rangle + \langle \phi_i \nabla p \rangle = \oint G \hat{n} \cdot \nabla \vec{u} \phi_i ds + \oint \frac{G}{1-2\nu} \hat{n} (\nabla \cdot \vec{u}) \phi_i ds \quad (3a)$$

$$\langle k \nabla p \cdot \nabla \phi_i \rangle = \oint k \hat{n} \cdot \nabla p \phi_i ds \quad (3b)$$

In these expressions,  $\langle * \rangle$  represents integration over the domain of the problem. Also,  $\phi_i$ , is the  $i$ th member of the standard  $C^0$  local Lagrange polynomial interpolants associated with finite elements [14].  $\oint *$  represents integration over the contained boundary and  $\hat{n}$  is the outward-pointing normal to the enclosed boundary. The spatial discretization of (3a) and (3b) is concluded using the Galerkin method in order to expand the unknown fluid pressure,  $p$ , and the unknown displacement vector,  $\vec{u}$ . These are represented as the summation of unknown coefficients, which vary spatially, that are multiplied by known functions of position [14], [16].

$$\vec{u}(\vec{x}) = \sum_j \vec{u}_j \phi_j(\vec{x}) \quad (4a)$$

$$p(\vec{x}) = \sum_j p_j \phi_j(\vec{x}) \quad (4b)$$

The spatially discretized, set of ordinary differential equations are:

$$\sum_j \vec{u}_j \langle G \nabla \phi_j \cdot \nabla \phi_i \rangle + \sum_j \vec{u}_j \cdot \left\langle \nabla \phi_j \frac{G}{1-2\nu} \nabla \phi_i \right\rangle + \sum_j p_j \langle \nabla \phi_j \phi_i \rangle = \oint G \hat{n} \cdot \nabla \vec{u} \phi_i ds + \oint \frac{G}{1-2\nu} \hat{n} (\nabla \cdot \vec{u}) \phi_i ds \quad (5a)$$

$$\sum_j p_j \langle k \nabla \phi_j \cdot \nabla \phi_i \rangle = \oint k \hat{n} \cdot \nabla p \phi_i ds \quad (5b)$$

In Cartesian coordinates, equations (5a) and (5b) can be represented in matrix form.

$$[A]\{U\} = \{B\} \quad (6)$$

In this matrix expression, (6),  $[A]$  consists of submatrices built from element integrations,  $\{U\}$  represents the unknown values of displacements and pressure, and  $\{B\}$  consists of known systems forcing and boundary conditions. The two-dimensional (2D) representation of the local element contribution to the global matrix representation is seen below.  $[A]$  is determined for each weighted residual equation and concerned coefficient as seen in (7a), and  $\{U\}$  and  $\{B\}$  are the  $j^{\text{th}}$  set of coefficients and known forcing conditions as defined by (7b) and (7c) respectively.

$$[A]_{ij} = \begin{bmatrix} G \left\langle \frac{2(1-\nu)}{1-2\nu} \frac{d\phi_j}{dx} \frac{d\phi_i}{dx} + \frac{d\phi_j}{dy} \frac{d\phi_i}{dy} \right\rangle & G \left\langle \frac{2\nu}{1-2\nu} \frac{d\phi_j}{dy} \frac{d\phi_i}{dx} + \frac{d\phi_j}{dx} \frac{d\phi_i}{dy} \right\rangle & \left\langle \frac{d\phi_j}{dx} \phi_i \right\rangle \\ G \left\langle \frac{2\nu}{1-2\nu} \frac{d\phi_j}{dx} \frac{d\phi_i}{dy} + \frac{d\phi_j}{dy} \frac{d\phi_i}{dx} \right\rangle & G \left\langle \frac{2(1-\nu)}{1-2\nu} \frac{d\phi_j}{dy} \frac{d\phi_i}{dy} + \frac{d\phi_j}{dx} \frac{d\phi_i}{dx} \right\rangle & \left\langle \frac{d\phi_j}{dy} \phi_i \right\rangle \\ \langle 0 \rangle & \langle 0 \rangle & k \left\langle \frac{d\phi_j}{dx} \frac{d\phi_i}{dx} + \frac{d\phi_j}{dy} \frac{d\phi_i}{dy} \right\rangle \end{bmatrix} \quad (7a)$$

$$\{U\}_j = \begin{bmatrix} u_{x_j}(t_n) \\ u_{y_j}(t_n) \\ p_j(t_n) \end{bmatrix} \quad (7b)$$

$$\{B\}_j = \begin{bmatrix} \hat{x} \cdot \oint \sigma_s(t_n) \cdot \hat{n} \phi_i ds \\ \hat{y} \cdot \oint \sigma_s(t_n) \cdot \hat{n} \phi_i ds \\ \oint k \nabla p(t_n) \cdot \hat{n} \phi_i ds \end{bmatrix} \quad (7c)$$

We should note that the expressions shown in Equation (7a-c) readily extend to three dimensions using basis functions associated with tetrahedral elements [16]. These discretized matrix representations were used for all ICH evacuation models, namely, the element-deletion model, and superposition approach (described in Sections 2.4 and 2.5, respectively).

## 2.2 Analytical Validation of Two and Three Dimensional Models

To validate the accuracy of the biphasic, poro-elastic model in this work, a 2D and 3D mesh were generated and their solutions were compared to a one-dimensional (1D) analytical solution of an equivalent domain, with the same boundary conditions (BCs). The dimensions are shown in Figure 1.

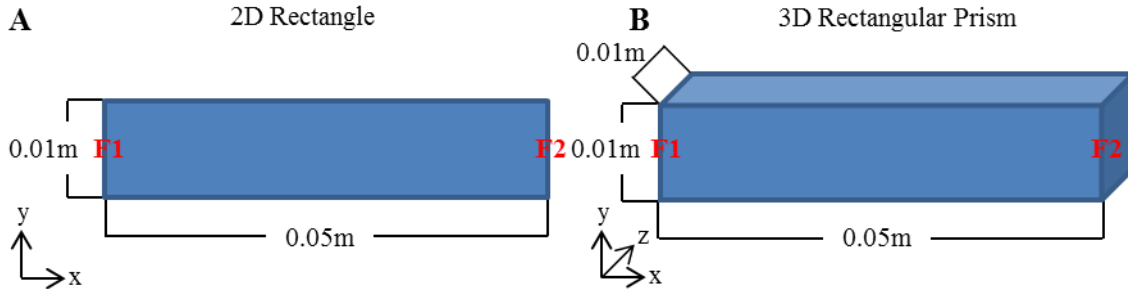


**Figure 1.** For the validation of the model, two meshes were generated. Panel A represents the dimensions of the 2D mesh used to validate the 2D FEM solution. Panel B represents the dimensions of the 3D, rectangular prism mesh used to validate the 3D FEM solution. F1 and F2 indicate face 1 and face 2 respectively. The arrows indicate the axes directions for x, y, and z in Cartesian coordinates. The origin is in the bottom left corner for both meshes.

With respect to the simulation, the BC on the left side assumes that pressure and displacement is equal to zero. On the right hand side ( $x=0.05$  m), it is assumed that the pressure is equal to 1333 Pascals (Pa), and the BC associated with solid matrix is stress free. The equations associated with (2a) and (2b) can be reduced to equations (9a) and (9b) in 1D. Using the BCs provided above, an analytical solution for pressure and displacement comparisons can be determined for comparison and is shown in equations (10a) and (10b), respectively. In these equations  $E$  is elastic modulus, and  $P_o$  is the value of pressure applied (1333 Pa).

$$E \frac{\partial^2 \vec{u}}{\partial x^2} - \frac{\partial p}{\partial x} = 0 \quad (9a)$$

$$\frac{\partial^2 p}{\partial x^2} = 0 \quad (9b)$$

$$p(x) = \left( \frac{P_o}{0.05} \right) x \quad (10a)$$

$$\vec{u}(x) = \left( \frac{P_o}{2E(0.05)} \right) x^2 + \frac{-P_o}{E} x \quad (10b)$$

For the 2D FEM comparison, the rectangular mesh, illustrated in Figure 1A, was governed by the equations (5a) and (5b). Using Dirichlet BCs, at face 1 (F1), pressures and displacements were set to zero. At face 2 (F2), using Dirichlet BCs, the pressure values were set equal to 1333 Pa, while conditions on the elastic matrix were stress free. BCs associated with top and bottom of the domain are allowed to slide along the wall in the  $x$ -axis direction, but are prohibited from displacing in the  $y$ -axis direction. BCs similar to the 2D framework were used in the 3D simulation. The elastic modulus ( $E$ ) is 2100 Pa for both the 2D and 3D comparisons. In order to make the 2D and 3D approximations similar to the 1D analytical solution, the Poisson's ratio value is 0. For validation, the displacement and pressure values at a distance from the origin are compared.

## 2.3 Common Model Properties for the ICH Evacuation Representations

There are three representations of ICH evacuation presented in this work. They differ in how evacuation is represented with respect to applied boundary conditions, but their core structure is common. For the sake of discussion, these are referred to as the central evacuation representation (Section 2.4 below) and the superposition evacuation representations (1) and (2) (Section 2.5 below). They were evaluated in 2D. All models were constructed on a FEM, fixed grid, and governed by Equations (2a) and (2b). The matrices associated with Equations (6), (7a), (7b), and (7c) were constructed based on a predefined brain mesh, which is illustrated in Figure 2. The elastic modulus of the brain parenchyma,

ventricles, and ICH are 2100 Pa, 1Pa, and 1050 Pa respectively. The Poisson's ratio ( $\nu$ ) is 0.45. The hydraulic conductivity constant for the brain parenchyma /ICH and ventricles are  $1 \times 10^{-7}$  m<sup>3</sup>/s/kg and  $1 \times 10^{-3}$  m<sup>3</sup>/s/kg respectively. Along the skull boundary, which is the outermost limit of the mesh, Dirichlet BCs were used to set the pressure and displacements equal to zero. This represents the skull constraints on the brain and defining the pressure at the skull as zero relative to the applied evacuation pressure. The sole difference between the representations of ICH evacuation is how the evacuation is applied computationally, which is illustrated in Figure 2A and 2B. These will be outlined in Sections 2.4 and 2.5.

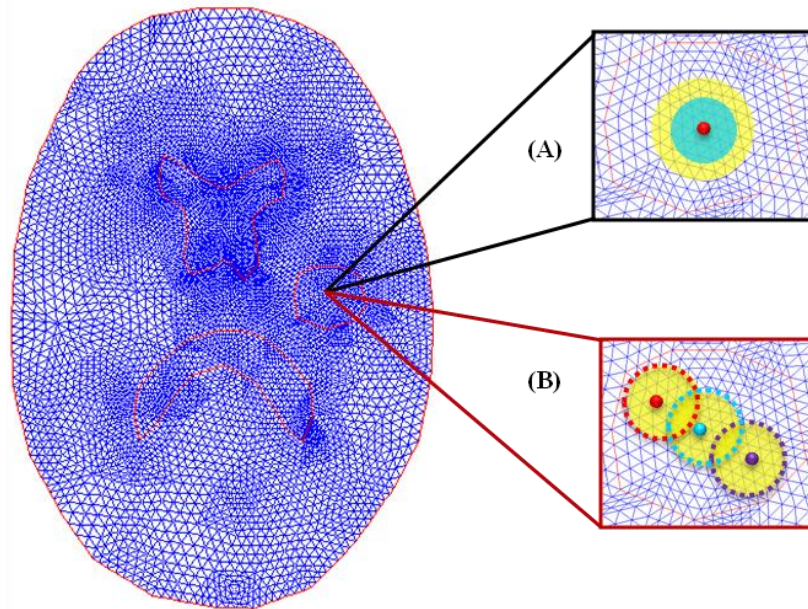


**Figure 2.** This figure displays the three models being tested on a brain mesh. (A) represents the deployment of pressure in the central evacuation representation of ICH evacuation. (B) represents the deployment of pressure in both superposition evacuation representations of ICH evacuation. The outermost boundary of the mesh represents the skull. The two asymmetric, internal boundaries represent the brain's ventricles. The circular portion of the mesh, which is also displayed in the details, represents the ICH.

#### 2.4 Two-Dimensional, Central Evacuation Representation

The behavior of the central ICH evacuation is visualized in Figure 2A. Generally, in this representation, the net aspiration of the cannula is treated as a source originated from the center of the ICH, which produces an increasingly larger cavity as material is removed. At the completion of consecutive iterations, the final evacuated cavity can be estimated. In the central evacuation representation, the pressure of the cannula is treated as a Dirichlet BC with magnitude equaling the applied pressure. In this simulation, the magnitude of the pressure was selected to be -1333 Pa. A total of three iterations were completed in this simulation, where each iteration represents one complete application of the cannula. During the first iteration, the application of the cannula is represented by a single, Dirichlet BC at a single node (red dot in Figure 2A). After this, the pressure, displacement, and von Mises stress distribution are calculated. The von Mises stress distribution, calculated per element, was used as the failure criterion in order to determine if an element, which represents a section of tissue, was flagged for deletion. Due to the lack of experimental data, the yield criteria for the three materials are determined empirically during the first iteration of this procedure. The yield criterion for the ICH was set to be 0.95 times the maximum von Mises stress calculated in the ICH during this first iteration. The yield criterion for the brain and ventricles are set as 10 times the maximum von Mises stress of the brain and ventricles respectively calculated during the first iteration. This is representative of the ICH being evacuated more readily than the other tissue types. These yield criteria were selected to effectively demonstrate the behavior of this evacuation representation. In order to accurately select a yield criterion, an empirical investigation would be needed; but as the purpose of this simulation study is to just understand performance differences under similar conditions, it is not needed here. If the elements were flagged for deletion (stress higher than criterion), they were removed from the solver by not

including them in the next construction of the matrices, while leaving the un-evacuated mesh intact. Moving into the next iteration, during the matrix assembly, elements which were evacuated during the previous iteration were not built, effectively removing their influence from the solution of the iteration. The new boundary of the evacuated cavity, represented by the blue circle in Figure 2A is where the applied pressure is now redeployed during the second iteration. This represents the remaining tissue migrating towards the cannula during the second iteration, and the pressure applied from the cannula now deployed over a greater area. This is enforced using Dirichlet boundary conditions. Upon completion of the second iteration, the displacement, pressure, and von Mises stress distributions are once again calculated, and a new list of deleted elements, representing evacuated tissue, is generated using the previously calculated yield criterions. Entering the final iteration, the same process is repeated. The elements which were flagged for deletion are not included in the matrix assembly, and the pressure applied by the cannula is now deployed over the outer boundary of the new evacuated cavity, as seen by the yellow circle in Figure 2A. This method requires the recalculation of the  $[A]$  matrix (Equation 6) every iteration due to the elimination of element contributions and the redeployment of Dirichlet boundary conditions in new regions of the mesh. In this simulation, only three iterations were conducted, but this general process can be performed as many times as necessary, capturing the entire evacuation process.

### 2.5 Two-Dimensional, Superposition Evacuation Representation

The behavior of the superposition evacuation of an ICH is visualized in Figure 2B. The motivation of this representation is that during the evacuation procedure, the cannula is moving along a preplanned path. Rather than capturing the net evacuation, as done with the central evacuation representation, this method follows the cannula along its preplanned path. Each location within its trajectory is treated as one complete application of the cannula, and at the completion of one application, the model moves to the next location as dictated by the surgical plan. At the completion of the path, the total evacuated cavity can be estimated by superimposing the separate evacuation solutions. In this presented simulation, a total of three cannula applications are performed at three different cannula locations. Unlike the central evacuation, each suction is treated as a volumetric sink with an empirically determined magnitude to engender pressures in the mesh equivalent to -1333 Pa. This representation was approached two ways, superposition representation (1) and superposition representation (2).

In superposition representation (1), during the first iteration, represented by the red dot in Figure 2B, the cannula is deployed on a node as a volumetric sink. Using this, the model was solved for the first iteration and pressure, displacement, and von Mises stress distributions were calculated and stored. Using von Mises stress as the failure criterion, elements, representative of tissue, are flagged for deletion. Similar to the central evacuation representation, the von Mises yield criterion is empirically determined based on the stress distribution calculated during the first iteration. In a similar manner to the central evacuation method, in order to illustrate the behavior of this evacuation method, the yield criterion for the ICH was selected as 0.75 times the maximum von Mises stress of the ICH. The yield criterion of the brain and ventricles are selected as 10 times the maximum von Mises stress in both materials respectively. These values are stored and used as the yield criterion for all three material types during the simulation. The list of elements that were deleted after the first cannula deployment are stored, and the evacuated cavity of this suction can be visualized by the dashed red line in Figure 2B. Moving onto the second iteration, the cannula location is moved to its second position, and the same volumetric sink is applied on this node. This is visualized in Figure 2B as the light blue dot. Then the model is solved to estimate pressures, displacements, and von Mises stresses, and these solutions are stored. The tissue evacuated as the result of the second iteration is stored, and this evacuation is visualized by the light blue dashed circle in Figure 2B. Moving onto the final iteration, the same process is repeated. The cannula is moved to its third location and is visualized as the purple dot on Figure 2B. The elements deleted due to this iteration are shown by the purple dashed line in Figure 2B. This process can be repeated indefinitely, as required to appropriately represent the path of the cannula during the ICH evacuation. The final estimated evacuated cavity is formed by determining the outer contours resulting from the superposition of the elements flagged for deletion during all three iterations performed. This is done by adding the three results together. This is illustrated by the yellow shape in Figure 2B. This method only requires the  $[A]$  matrix (Equation 6) to be factored once, since each iteration is independent of each other and representations of aspiration are based on right-hand-side equation adjustments only.

In superposition representation (2), rather than solving three iterations of the model for pressure, displacement, and von Mises stresses, only one iteration is performed. This further simplification of the superposition representation requires the formation and factorization of the  $[A]$  matrix once. Then, using a series of volumetric sinks, the  $\{B\}$  vector (Equation 6) is populated with three conditions representing the same three deployments of the cannula. This reflects a path the

cannula would travel in the surgical procedure. The deployment of these sinks is visualized as the red, blue, and purple dots in Figure 2B. Using this, the model was solved for the first iteration and pressure, displacement, and von Mises stress distributions were calculated and stored. The yield criterion for the ICH was selected as 0.75 times the maximum von Mises stress of the ICH material during this single iteration. The yield criterion of the brain and ventricles are selected as 10 times the maximum von Mises stress in both materials respectively. The deleted cavity is solved in a single iteration and is visualized by the yellow shape in Figure 2B. Superposition representation (2) can be modified by altering the number of and location of the volumetric sinks enforced, thereby representing different cannula trajectories within the surgical plan.

### 2.6 Three-Dimensional, Continuum, Finite Element Model of Brain Deformations

As a preliminary study into applying the evacuation methods in 3D, an example mesh of a human brain with an artificial ICH was made using a custom-built mesh generator and consisted of 21076 nodes and 113183 linear tetrahedral elements. The material properties selected for this mesh were 2100 Pa for the elastic modulus of the brain, 1050 Pa for the elastic modulus of the ICH, and 0.45 for the Poisson's ratio of both materials. Also, the hydraulic conductivity was set uniformly as  $1 \text{ m}^3/\text{s}/\text{kg}$  for the entire mesh, which is appropriate given the nature of the equations. The shear modulus ( $G$ ) value is defined such that  $G = E / (2 * (1 + \nu))$ . The governing equations were the same as the 2D case, Equations (2a) and (2b). The boundary conditions used to solve this 3D representation take into consideration the outermost boundary of the brain mesh, which represents the boundary of the brain with the skull. The first condition is that there is no displacement at the skull. This is enforced using Dirichlet boundary conditions, setting displacements in the normal and tangential directions to be equal to zero. The second condition, is that the pressure at this boundary is 0 Pa, and is applied as Dirichlet boundary conditions. To represent the applied suction, the magnitude of pressure, -1333 Pa, was applied on the four nodes of one tetrahedral element contained within the artificial ICH. This entire simulation is representative of applying a single suction to the ICH. At the completion of this simulation, displacements and pressures were estimated for each node.

## III. RESULTS

### 3.1 Analytical Validation Results

The continuum, finite element model of brain deformations were solved in 2D and 3D and compared to the analytical 1D solution. They were simulated using the same material properties, dimensions, and constraints. The results of the 2D solution are shown in Figure 3. Figure 3A shows the overlay of the model solution and the analytical solution for displacement, and reflects that the solutions are in agreement. The relative average displacement error is less than 1% over the entire domain. Figure 3B overlays the analytical solution and the model solution for pressure, and reflects that the relative pressure error is less than 1%.

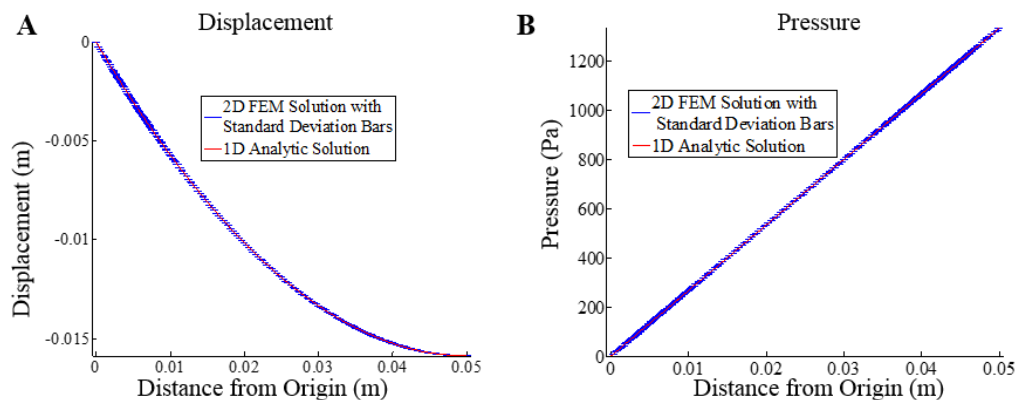


**Figure 3.** Comparison of the 2D finite element model solution in a rectangular mesh to a 1D analytical solution. Panel A represents the displacement along the primary axis, and panel B represents the pressure at the corresponding locations. The error bars represent the standard deviation at each point. The relative average displacement and relative pressure error are both less than 1%.

The results of the 3D validation are shown in Figure 4. In Figure 4A, the 3D displacement FEM solution is overlaid with the 1D analytical solution of displacement, with relative average displacement error less than 1%. In Figure 4B, the 3D FEM solution for pressure is overlaid with the 1D analytical solution, and the relative pressure error is less than 1%.

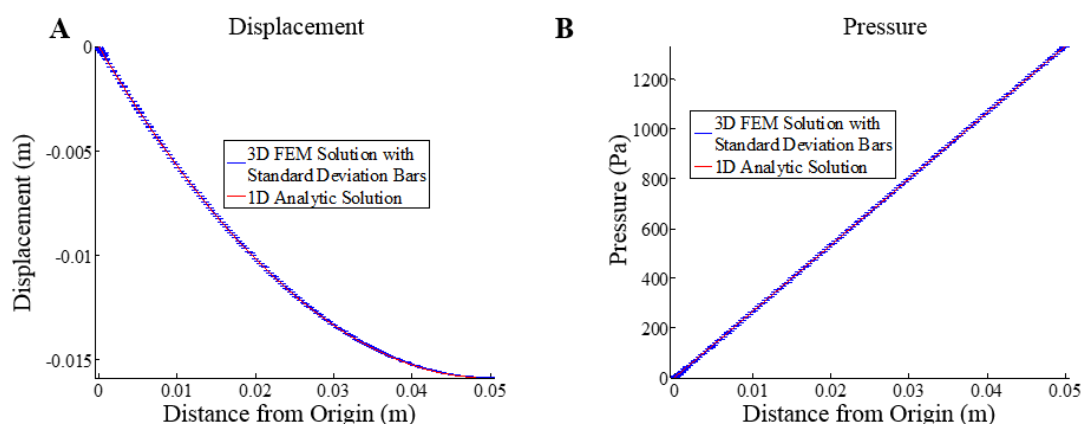


**Figure 4.** Comparison of the 3D finite element model solution in a rectangular prism to a 1D analytical solution. Panel A represents the displacement in the primary axis, and panel B represents the pressure at the corresponding locations. The error bars represent the standard deviation at each point. The relative average displacement and relative pressure error are both less than 1%.

### 3.2 Comparison of the Evacuation Methods

A table summarizing the results from the model solutions is below.

Model	Percent ICH Evacuation	Percent Brain Evacuation	Computational Burden - LU Factorization	Back Substitution for Solution	Total Cost
Central Evacuation	100.00%	0.51%	$\sim 3 * O(B^2 \cdot N)$	$3 * N^2$	$\sim 3B^2 \cdot N + 3N^2$
Superposition Evacuation (1)	14.50%	0.00%	$O(B^2 \cdot N)$	$3 * N^2$	$\sim B^2 \cdot N + 3N^2$
Superposition Evacuation (2)	18.90%	0.00%	$O(B^2 \cdot N)$	$N^2$	$B^2 \cdot N + N^2$

**Table 1.** Comparison of the three 2D representations of ICH evacuation in the same finite element mesh. This is a summary of how all three representations compare in reference to the percent of ICH evacuated, percent of brain parenchyma evacuated, the computational burden associated with the LU factorization, and the computational burden associated with the back substitution for the solution.  $B$  is bandwidth, and  $N$  is the number of unknowns.

As described in Sections 2.4 and 2.5, the difference between the central evacuation representation, superposition evacuation representation (1), and superposition evacuation representation (2) of ICH aspiration is how the volumetric sinks create the aspiration condition resulting from the cannula within the model. In the simulations of the central evacuation (Figure 5, Panels A-C), the superposition evacuation (1) (Figure 5, Panels D-F), and the superposition evacuation (2) (Figure 5, Panels G-I) represented in Figure 5, three volumetric sinks representing three cannula applications, were applied in all three scenarios. All panels are representative of the evacuation after the deployment of three sets of pressure boundary conditions, and from a qualitative observation, they exhibit dissimilar behavior. After three iterations, the percent of the ICH evacuated in the central evacuation method is 100%, and the percent of brain parenchyma evacuated is 0.51% (Table 1). After three iterations, in the superposition evacuation method (1), the percent of the ICH evacuated is 14.5%, and no brain parenchyma was evacuated (Table 1). After the single deployment of three pressures in the superposition evacuation method (2), the percent of the ICH evacuated is 18.90%, and no brain parenchyma was evacuated (Table 1). All three methods were able to identify the removal of ICH tissue, calculate

pressure (Figure 5, Panels A, D, and G) and displacements at every node, and estimate the von Mises stress per element (Figure 5, Panels B, E, and H). Additionally, they capture the bulk deformation of the surrounding tissue towards the area of evacuation (Figure 5, Panels C, F, and I).

A significant difference between the evacuation methods is the computational burden involved with their executions (Table 1). All three models presented involve approximately the same memory allocation. They differ significantly in matrix assembly and the number of operations required. For memory efficiency, lower upper (LU) decomposition can be used. The factoring of matrix  $[A]$  (Equation 6) is the most computational expensive step in calculating the solution of the models [16]. The computational burden involved in factorization is  $O(B^2 \cdot N)$ , where  $B$  is the bandwidth of the  $[A]$  matrix, and  $N$  is the number of unknowns being solved for [16]. Both  $B$  and  $N$  are the same in the three models. The central evacuation representation, however, redefines the  $[A]$  matrix every iteration. This means that the computational burden in factorization is approximately  $3 * O(B^2 \cdot N)$ . On the other hand, both superposition representations only requires the construction of one  $[A]$  matrix used for all iterations. Therefore the total computational burden of factorization is only  $O(B^2 \cdot N)$ . The 3 fold increase in computational burden for the central evacuation coupled with the need to rebuild the  $[A]$  matrix is a significant limitation versus the other methods. Even in the case where only local regions where evacuations are occurring and only small changes to the global  $[A]$  matrix were needed, it would still require storing an addition  $[A]$  matrix to accommodate this process. Ultimately, Table 1 indicates some strong advantages for superposition methods.

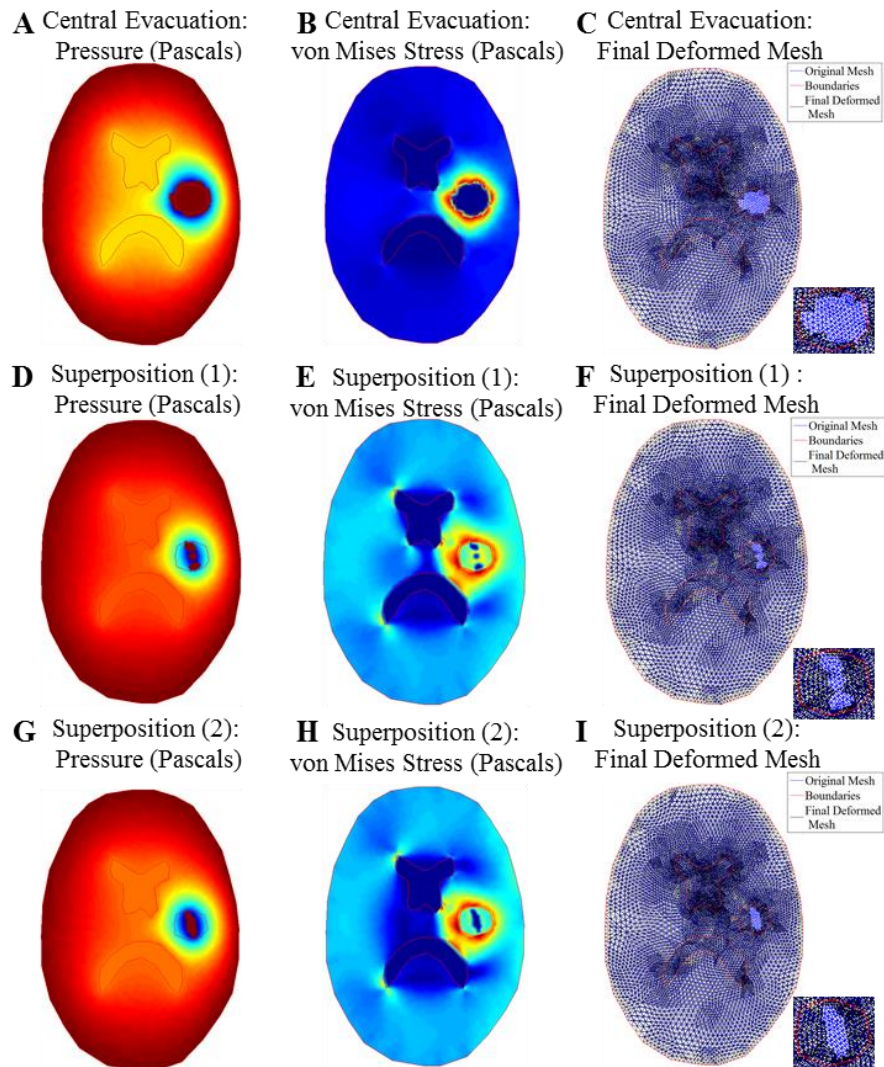


**Figure 5.** Comparison of the three representations ICH evacuation in the same finite element mesh. The top row (A-C) is the central evacuation model solution after the completion of three iterations. The middle row (D-F) is the superposition model (1) solution after adding the solutions of the three iterations together. The bottom row (G-I) is the superposition model (2) solution after a single iteration containing three applied pressure sources. A, D, and G represent the pressure distribution throughout the mesh, where cooler colors indicate larger negative pressures, warmer colors indicate less negative pressures, and maroon indicates deleted elements. B, E, and H represent the von Mises stress distribution, where warmer colors indicate higher positive von Mises stresses, cooler colors indicate smaller von Mises stresses, and dark blue indicates zero stresses and evacuated elements. C, F, and I show the change in mesh structure from its initial configuration point (blue) to its final deformed state (black). On the bottom right of C, F, and I is an enlarged view of the ICH.

### 3.3 Preliminary Three-Dimensional Model

The results of the 3D FEM model solution are shown in Figure 6. In both panels, the magenta lines visualize the brain mesh and artificial ICH used in this simulation. The cannula's pressure was deployed within the ICH, and solutions for displacement and pressure were estimated at all nodes within the mesh in this 3D simulation. A slice through the brain, near the location of the cannula deployment is shown in Figure 6. In Figure 6A, it is evident that the bulk of the motion occurs closest to the location of pressure deployment. Similarly, in Figure 6B, the highest pressures are at the location of the cannula. This is qualitatively the same behavior seen in the 2D model, and is indicative of the 3D model being viable for ICH evacuation solutions.

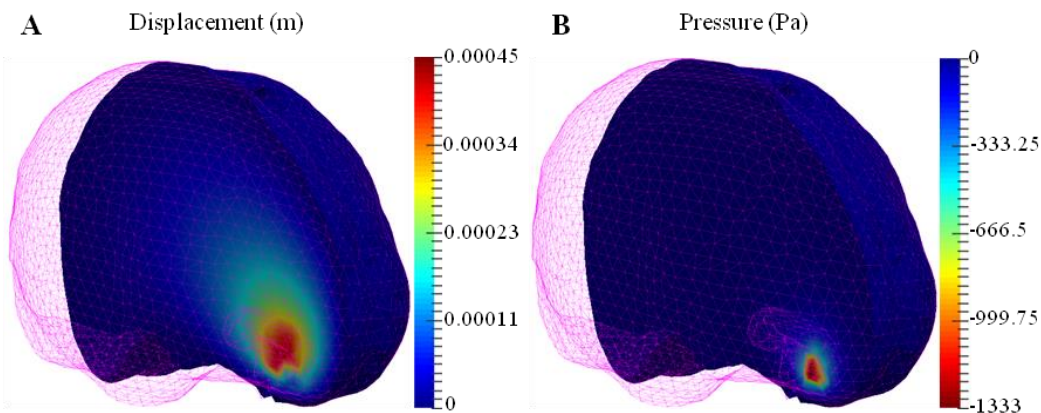


**Figure 6.** For these simulations, a pressure of -1333 Pa was placed within the ICH. Panel A is a slice through the 3D brain mesh, representing the displacement solution. Panel B is a slice through the 3D brain mesh, representing the pressure solution.

## IV. DISCUSSION

The overall goal of this study was to develop a model to estimate the aspiration of an ICH using a needle-based robotic system for image-guided evacuation of ICHs. Interpreting the results of the 2D and 3D simulations performed, the relative average errors between the analytical solution and the FEM solution were less than 1%. These errors are acceptable, indicating the acceptability of the steady-state model used to solve for ICH evacuation in 2D. Minor discrepancies between the model solutions and the analytical solutions, seen in Figures 3 and 4, may be the result of the numerical error due to resolution of the mesh used in the solution. The accuracy of the model solutions, both in 2D and 3D, support its use as a means to capture steady-state brain deformation and pressure in a model of ICH evacuation. An additional improvement could be obtained through the incorporation of the temporal aspect of the equations for consolidation in soft-tissue, shown in Equations (1a) and (1b).

Comparing the 2D models used to estimate the deformations, there are several evident trends. There are substantial differences in the representation of the cannula between the central evacuation representation and both of the superposition evacuation representations. The amount of ICH removed after three pressure deployments was

significantly different; however all models were able to capture the removal of an ICH, indicate if brain parenchyma was evacuated, and estimate the distribution of pressure and displacements. The advantage of the central evacuation representation is that it only relies on knowing the applied evacuation and the node approximately in the center of the ICH. However, while intuitive with respect to application, it would require special care with respect to failure criterion to maintain stability. More specifically, as elements that violate the von Mises criterion are eliminated, simply just reapplying the pressure leads to increasing forces due to increased area exposure. To prevent this, the use of a dynamic grid and an alternative failure criterion is likely needed. The superposition evacuation representation, both (1) and (2), do not have this problem as they are calculated on a fixed grid. In addition, they enable incorporating knowledge of the cannula's path during ICH aspiration. They are also likely more adaptable to other ICH evacuation methods that may have different approaches. Even more importantly, the computational burden of superposition evacuation (1) and superposition evacuation (2) is significantly less than the central evacuation representation which may be a considerable advantage when translating to the intraoperative setting. A limitation of the superposition representation is its inability to accommodate the impact of continual removal during the aspiration process. Additionally, all three methods are limited by the use of the von Mises stress as a failure criterion for material evacuation. The method performance is dependent on the definition and number of successive cannula applications. This would undoubtedly require tuning to match biological conditions, and the extrapolation to novel brains may not be straight forward. This concept of empirical tuning of one of these basic biophysical models acting as a type of biophysical filter for ICH aspiration is intriguing and an area for future development.

The three-dimensional model solution is a first step towards implementing the approximations of ICH evacuation in a patient specific manner. By generating meshes from patient-specific, preoperative scans, ICH evacuation can be simulated using knowledge of the patient's physiology and the surgeon's therapeutic plan for evacuation. Moving forward, the second superposition representation of evacuation should be favored, due to its ability to more realistically reflect the surgical procedure and its decreased computational burden. In order to more fully validate the accuracy of the superposition evacuation representation (2), phantom studies will be needed. Generally, the results of our simulations indicate the feasibility of modeling ICH evacuation using finite element modeling, but further work into its development is needed.

## V. CONCLUSIONS

While the methods presented in this paper show aspects of promise, more work is needed in order to capture the complexity of ICH aspiration and its associated material failure criterion. The novelty of the work presented in this preliminary study is that to the best of our knowledge, it is the first computational model of ICH evacuation. Three methods of representing ICH evacuation were investigated, but the second superposition representation better accounts for the surgical environment behavior and is more readily incorporated into an intra-operative environment. Moving forward, following realization and validation of the 3D patient-specific model this framework research can be applied to the ICH robot system. It would enable the reduction of intra-operative CT scans used to ensure healthy tissue would not be aspirated. This work can also be applied to other minimally invasive techniques used in the brain for other aspiration based mechanisms.

## VI. ACKNOWLEDGEMENTS

This work is supported by the NIH-National Institute of Neurological Disorders and Stroke R01NS049251 and R21NS087796. This work was also supported by the Vanderbilt Institute in Surgery and Engineering Seed Grant program.

## VII. REFERENCES

- [1] van Asch, C. J. J., M. J. A. Luitse, G. J. E. Rinkel, I. van der Tweel, A. Algra, and C. J. M. Klijn, "Incidence, case fatality, and functional outcome of intracerebral haemorrhage over time, according to age, sex, and ethnic origin: a systematic review and meta-analysis," *Lancet Neurol.*, 9(2), pp. 167–176 (2010).
- [2] Elijovich, L., P. Patel, and J. Hemphill, "Intracerebral Hemorrhage," *Semin. Neurol.*, 28(5), p. 657 (2008).

- [3] Johnsen, S. P., L. Pedersen, S. Friis, W. J. Blot, J. K. McLaughlin, J. H. Olsen, and H. T. Sørensen, "Nonaspirin nonsteroidal anti-inflammatory drugs and risk of hospitalization for intracerebral hemorrhage: a population-based case-control study," *Stroke*, 34(2), pp. 387–391 (2003).
- [4] Anderson, C., E. Heeley, Y. Huang, J. Wang, C. Stapf, C. Delcourt, R. Lindley, T. Robinson, P. Lavados, B. Neal, J. Hata, H. Arima, M. Parsons, Y. Li, J. Wang, S. Heritier, L. Q. M. Woodward, R. Simes, S. Davis, J. Chalmers, "Rapid Blood-Pressure Lowering in Patients with Acute Intracerebral Hemorrhage," *N Engl J Med.*, 368(25), pp. 2355–2365 (2013).
- [5] Broderick, J., T. Brott, J. Duldner, T. Tomsick, and G. Huster, "Volume of Intracerebral Hemorrhage A Powerful and Easy-to-Use Predictor of 30-Day Mortality," *Stroke*, 24(7), pp. 987–93 (1993).
- [6] Murthy, J. M. K., G. V. S. Chowdary, T. V. R. K. Murthy, P. Syed Ameer Bhasha, and T. Jaishree Naryanan, "Decompressive Craniectomy With Clot Evacuation in Large Hemispheric Hypertensive Intracerebral Hemorrhage," *Neurocrit Care*, 2, pp. 258–262 (2005).
- [7] Newell, D. W., M. M. Shah, R. M. S. Wilcox, D. R. Hansmann, E. B. S. Melnychuck, J. S. M. Muschelli, and D. F. Hanely, "Minimally Invasive Evacuation of Spontaneous Intracerebral Hemorrhage Using Sonothrombolysis," *J. Neurosurg.*, 115(3), pp. 592–601 (2011).
- [8] Staykov, D., I. Wagner, B. Volbers, E. M. Hauer, A. Doerfler, S. Schwab, and J. Bardutzky, "Natural course of perihemorrhagic edema after intracerebral hemorrhage," *Stroke*, 42(9), pp. 2625–2629 (2011).
- [9] Burgner, J., P. J. Swaney, R. a. Lathrop, K. D. Weaver, and R. J. Webster, "Debulking from within: A robotic steerable cannula for intracerebral hemorrhage evacuation," *IEEE Trans. Biomed. Eng.*, 60(9), pp. 2567–2575 (2013).
- [10] Dupont, P. E., J. Lock, B. Itkowitz, and E. Butler, "Design and Control of Concentric-Tube Robots," *IEEE Trans. Robot.*, 26(2), pp. 209–225 (2010).
- [11] Takizawa, H., K. Sugiura, M. Baba, and J. D. Miller, "Analysis of intracerebral hematoma shapes by numerical computer simulation using the finite element method.," *Neurol. Med. Chir. (Tokyo).*, 34, pp. 65–69 (1994).
- [12] Miga, M. I., D. W. Roberts, F. E. Kennedy, L. A. Platenik, A. Hartov, K. E. Lunn, and K. D. Paulsen, "Modeling of retraction and resection for intraoperative updating of images," *Neurosurgery*, 49(1), pp. 75–85 (2001).
- [13] Sun, K., T. S. Pheiffer, A. L. Simpson, J. A. Weis, R. C. Thompson, and M. I. Miga, "Near Real-Time Computer Assisted Surgery for Brain Shift Correction Using Biomechanical Models," *IEEE J. Transl. Eng. Heal. Med.*, 2, pp. 1–13 (2014).
- [14] Paulsen, K. D., M. I. Miga, F. E. Kennedy, P. Jack Hoopes, A. Hartov, and D. W. Roberts, "A computational model for tracking subsurface tissue deformation during stereotactic neurosurgery," *IEEE Trans. Biomed. Eng.*, 46(2), pp. 213–225 (1999).
- [15] Biot, M. a., "General theory of three-dimensional consolidation," *J. Appl. Phys.*, 12(2), pp. 155–164 (1941).
- [16] Lynch, D. R., [Numerical Partial Differential Equations of Environmental Scientists and Engineering]. New York, NY: Springer Science+Business Media, Inc, (2005).